*Research Article*

# Study on the Mechanism of Compound Kidney-Invigorating Granule for Osteoporosis based on Network Pharmacology and Experimental Verification

**Hao Lv** [ID],[1] **Jiuxiang Wang** [ID],[1] **Yujun Zhu** [ID],[2] **and Ting Jiang** [ID][1]

[1]*The First Affiliated Hospital of Anhui University of Chinese Medicine, Hefei 230031, China*
[2]*Anhui University of Chinese Medicine, Hefei 230031, China*

Correspondence should be addressed to Ting Jiang; jiangting70@163.com

*Background*. This study used a combination of network pharmacology and experimental confirmation to clarify the mechanism of the compound kidney-invigorating granule (CKG) in treating osteoporosis (OP). *Methods*. The main bioactive compounds and corresponding targets of CKG were collected and screened via the Traditional Chinese Medicine Systems Pharmacology Database and Analysis Platform (TCMSP), Yet another Traditional Chinese Medicine (YaTCM), and UniProt databases. Disease targets of OP were summarized in GeneCards and the Comparative Toxicogenomics Database (CTD). Targets of CKG for OP were obtained by Venn diagram. The protein-protein interaction (PPI) network was constructed by the STRING database and then screened for hub genes through Cytoscape 3.7.2 software. The Gene Ontology (GO) and the Kyoto Encyclopedia of Genes and Genomes (KEGG) enrichment were analyzed and visualized by R software. Then, CB-Dock was used for molecular docking verification. Finally, we confirmed the antiosteoporosis effect of CKG through animal and cell experiments. *Results*. A total of 250 putative targets were obtained from 65 bioactive compounds in CKG. Among them, 140 targets were related to OP. Topological analysis of the PPI network yielded 23 hub genes. Enrichment analysis showed the targets of CKG in treating OP might concentrate on the MAPK signaling pathway, the TNF signaling pathway, the PI3K-Akt signaling pathway, etc. The results of molecular docking showed the bioactive components in CKG had good binding ability with the key targets. The experimental results showed that CKG-medicated serum had a promoting effect on proliferating hBMSCs, increasing the expression of AKT, PI3K, ERK1, and IkB in cells and decreasing the expression of IKK in cells. *Conclusion*. CKG has a complex of multicomponent, multitarget, and multipathway. This study lays the theoretical foundation for further *in vitro* and *in vivo* experimental studies and further expands the clinical applications of CKG.

## 1. Introduction

Osteoporosis (OP) is a systemic metabolic bone disease characterized by low bone mass, low bone density, and bone microstructure destruction, which leads to increased bone fragility and susceptibility to bone fracture. OP is considered a "silent disease" since it progresses without symptoms until a fracture occurs [1]. In the 2010 U.S. census, around 10.2 million adults aged 50 and older were living with OP [2]. An estimated 10.9 million males are suffering from OP in China, while the number of females suffering from OP is 49.3 million [3]. The incidence of OP increases yearly with the aging of the general population. Current treatments for osteoporosis include bisphosphonates, raloxifene, calcium, and vitamin D [4]. Nevertheless, these approved drugs have also shown significant side effects, such as the increased risk of hypercalcemia and hypercalciuria due to long-term vitamin D supplementation [5]. Since bisphosphonates are incorporated within the bone matrix with high affinity, long-term treatment with bisphosphonates may lead to atypical

femur fractures [6]. Raloxifene is associated with adverse effects such as thromboembolism, pulmonary embolism, and cerebrovascular death [7].

Compared with Western medicine, traditional Chinese medicine (TCM) has unique advantages in treating OP, such as low cost, multilevel, and prominent curative effect. Therefore, TCM is gradually attracting considerable attention from the international medical community and is accepted by non-Chinese as an additional and alternative medical treatment for OP due to these characteristics. Clinically, OP is regarded as "bone atrophy" and "lack of bone marrow" in TCM. According to TCM syndrome differentiation, OP is divided into kidney Yang deficiency syndrome, blood stasis syndrome and kidney deficiency syndrome, blood stasis and Qi stagnation syndrome, liver and kidney Yin deficiency syndrome, spleen and kidney Yang deficiency, and asthenia of the spleen and stomach syndrome.

Compound kidney-invigorating granule (CKG) is a TCM formula commonly used at the First Affiliated Hospital of Anhui University of Chinese Medicine. CKG is an effective cure for the OP of blood stasis and kidney deficiency syndrome. It is composed of six kinds of traditional Chinese drugs, namely, Radix Astragali (RA, Huang-qi in Chinese), Radix Paeoniae Alba (RPA, Bai-shao in Chinese), Radix Cyathulae (RC, Chuan-niu-xi in Chinese), Herba Epimedii (HE, Yin-yang-huo in Chinese), Caulis Polygoni Multiflori (CPM, Ye-jiao-teng in Chinese), and Concha Ostreae (CO, Mu-li in Chinese). Preliminary clinical studies have shown that CKG can significantly improve the clinical symptoms, bone mineral density (BMD), and visual analog scale (VAS) in postmenopausal nonelderly patients with OP. There were no adverse reactions that occurred during the study, and there were no significant abnormalities in the safety observation index. Therefore, CKG is safe and effective in treating postmenopausal nonelderly osteoporosis [8]. However, the pharmacological mechanism of CKG in treating OP is unknown.

TCM has become a significant source that provides potential lead compounds for drug development, especially those used to treat complex diseases, owing to its multicomponent and multitarget characteristics [9]. Guided by holistic thinking, TCM exerts unexpected curative effects in difficult and complicated diseases that Western medicine finds difficult to tackle [10]. However, due to the complex components of TCM prescriptions, traditional pharmacological methods to find out their unique actions through experiments may not be suitable for TCM research [11]. Western drug pharmacology molecular research may be stuck in a problem when applied to TCM prescriptions since it clarifies single or limited biological molecules from the perspective of reductionism instead of considering the overall theory of the organism [12]. On the contrary, network pharmacology uses the "target network, multi-components" research model to replace the traditional "one target, one drug" research model. Therefore, network pharmacology conforms to the core of the overall philosophy of TCM

[13]. This combination of pharmacokinetic evaluation and bioinformatics has made a significant contribution to the study of the molecular of TCM [14]. People apply the strategy to the pharmacological research of TCM compounds and explain the complex relationship between biological and herbal prescriptions [12]. Accordingly, regarding the unknown mechanism of CKG, this study adopted the method of network pharmacology to explore the molecular biology mechanism of CKG in treating OP.

The present study uses various platforms, databases, and tools to predict the bioactive compounds, potential targets, and pathways of CKG, aiming to explore the pharmacological network of CKG on OP and verify it through related experiments. Figure 1 shows the detailed technical strategy of the research.

## 2. Materials and Methods

### 2.1. Collection and Screening of Bioactive Ingredients.
The bioactive ingredients of CKG were identified by the Traditional Chinese Medicine Systems Pharmacology Database and Analysis Platform (TCMSP) (https://tcmspw.com/tcmsp.php) [15]. It compensates the insufficient information in the Yet another Traditional Chinese Medicine (YaTCM) database (https://cadd.pharmacy.nankai.edu.cn/yatcm/home) [16]. Oral herbal medicines must overcome obstacles in absorption, distribution, metabolism, and excretion (ADME) to be effective. In this process, oral bioavailability (OB) is one of the most important pharmacokinetic parameters [17]. As a qualitative concept, drug-like quality (DL) is used in drug design for the evaluation of the drug ability of a molecule and is utilized to optimize the pharmacokinetics and properties of a drug [18]. This study chose $OB \geq 30\%$ and $DL \geq 0.18$ as the criteria for screening bioactive ingredients. The OB and DL indicators of each ingredient in CKG were retrieved from the TCMSP database.

### 2.2. Prediction of Drug Targets for CKG.
The protein targets of the screened bioactive ingredients of CKG were obtained from the TCMSP database. The obtained protein targets were converted into gene targets in the Universal Protein Resource (UniProt) database (https://www.uniprot.org/) [19], a comprehensive database of protein sequence and annotation data.

### 2.3. Construction of Drug-Compound-Target Network.
The obtained bioactive ingredients, gene targets, and herbs were entered into Cytoscape 3.7.2 software (https://www.cytoscape.org/) for data visualization and construction of the "D-C-T" network [20]. The network nodes represent the herbs, gene targets, or bioactive components, and the edges indicate their interaction.

### 2.4. Collection of Gene Targets for OP.
OP-related human gene targets were obtained from two databases: GeneCards (https://www.genecards.org/) and the comparative
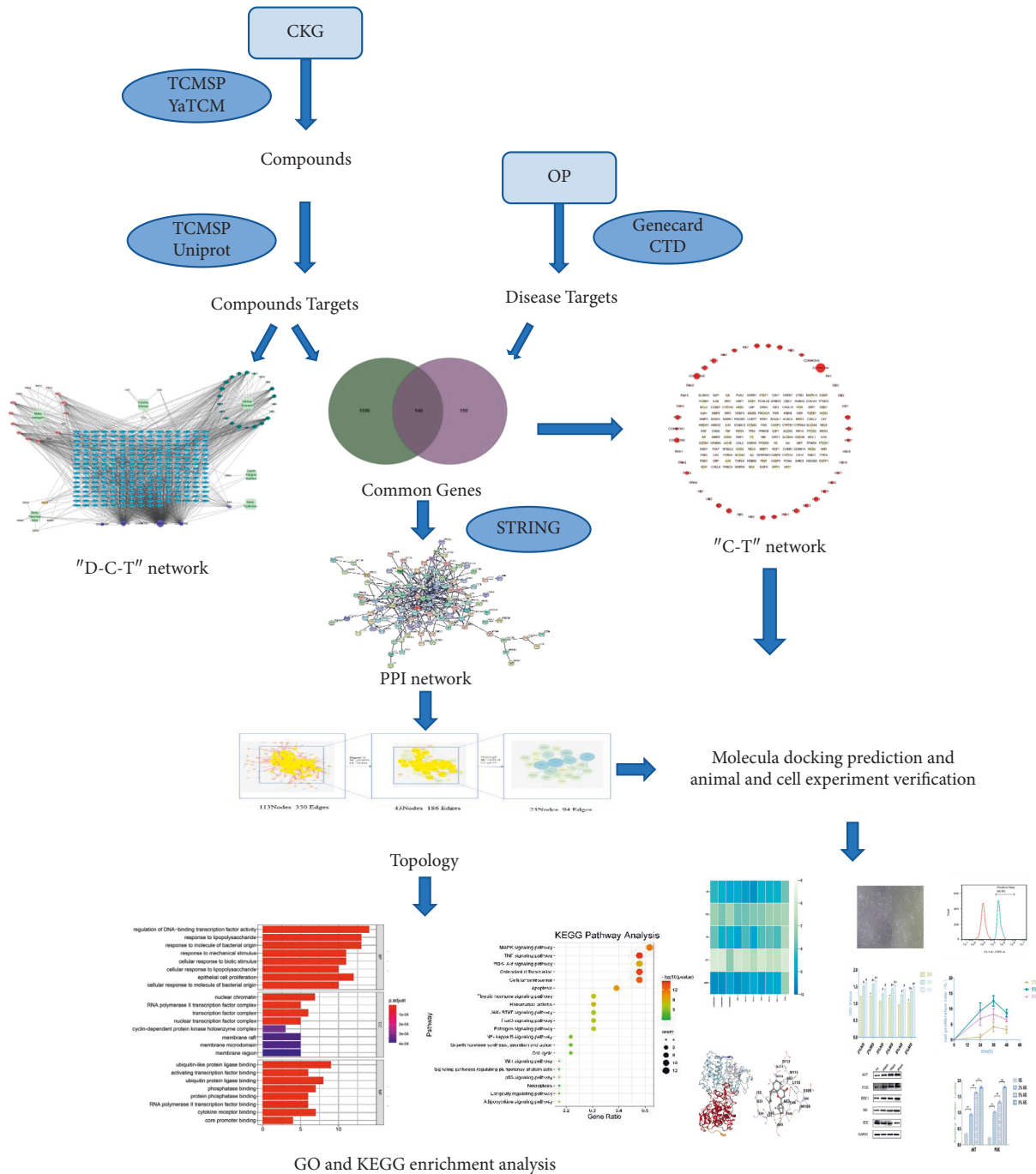
FIGURE 1: The technical strategy of the current study.

toxicogenomics (CTD) database (https://ctdbase.org/). The term "Osteoporosis" was used as the keyword for the search [21, 22].

*2.5. Collection of Relevant Targets for Formula Treatment of Diseases.* The results of gene targets of CKG were matched with the disease-associated genes of OP. The jvenn (https://www.bioinformatics.com.cn/static/others/jvenn/) was used to realize the visualization of the drug-disease

target and to draw Venn diagrams [23]. Then, the intersecting gene targets of CKG and OP were collected as the relevant targets of CKG for treating OP, which might be the potential target set of CKG in treating OP.

*2.6. Construction of a Compound-Target Network That Bioactive Ingredients of Formula with Intersecting Gene Targets.* The obtained bioactive ingredients and intersecting gene targets were imported into Cytoscape 3.7.2 software for

data visualization and construction of the "C-T" network. The nodes of the network represented the intersecting gene targets and bioactive components, and the edges indicated their interaction.

### 2.7. Protein-Protein Interaction (PPI) Network Construction and Core Gene Screening.

The common gene targets of CKG and OP were entered into the STRING database (https://string-db.org/) [24]. The selection parameter was set to "Homo sapiens" for species, the confidence level was set at 0.950 for the minimum required interaction score, and hid disconnected nodes in the network. The PPI network analysis results were downloaded in TSV format. The file was imported into Cytoscape software for topological property analysis. Then, this study evaluated the topological properties of the nodes in the interaction network by calculating three parameters, namely, "degree centrality (DC)," "betweenness centrality (BC)," and "closeness centrality (CC)" via the App CytoNCA [25]. These three parameters measure the importance of nodes in the network and indicate the nature of the nodes in the network. Nodes with high DC, BC, and CC implied that they were playing an essential role in the network. We obtained the core genes in the network by screening above the median value twice based on the results of the topological property analysis of PPI.

### 2.8. Gene Ontology (GO) and the Kyoto Encyclopedia of Genes and Genomes (KEGG) Enrichment Analysis.

Various bioinformatics analyses and visualization of the results can be achieved through the software R project (https://www.r-project.org/). Firstly, the ENSMBL gene ID of each core gene was obtained from RStudio, AnnotationHub, and org. Hs.eg.db, and then the GO function enrichment (molecular function, MF; biological process, BP; and cellular component, CC) and KEGG enrichment were enriched by RStudio, DOSE, and Cluster Profiler. In the programming language, pvalueCutoff = 0.05 and qvalueCutoff = 0.05 were set. The results of the analysis selected the top 10 items of BP, MF, and CC in GO enrichment and the top 20 filtered pathways most closely related to OP, then displayed the results of the GO enrichment analysis as a bar graph and the results of the KEGG enrichment analysis as a bubble graph.

### 2.9. Molecular Docking Verification.

Since there is no uniform standard for target screening of bioactive molecules, the 5 proteins with the highest degree of PPI network were selected for molecular docking with the 10 molecules with the highest degree of the "C-T" network. The bioactive compounds were downloaded as 2D structure files using the PubChem database (https://pubchem.ncbi.nlm.nih.gov/), converted into a 3D structure with ChemBio3D Ultra 14.0, and saved as a mol2 format file [26], whereas the RCSB PDB database (https://www.rcsb.org/) was used to retrieve and download the files in "PDB" format of the core target proteins [27]. Then, the proteins and molecules files were imported into the CB-Dock website (https://clab.labshare.cn/cb-dock/php/index.php) for molecular docking. Finally, the docking model with the lowest binding energy was selected and visualized.

### 2.10. Experimental Verification

#### 2.10.1. Materials

(1) Medicinal Materials. All Chinese medicines of CKG were purchased from the First Affiliated Hospital of Anhui University of Traditional Chinese Medicine. The prescription medicinal materials of each dose of CKG are HE (20 g), RC (15 g), RA (18 g), CO (10 g), RPA (20 g), and CPM (25 g), 30 doses in total.

(2) Antibodies and Reagents. The following antibodies and reagents were used for this study: high-glucose Dulbecco minimum essential medium (HG-DMEM) and fetal bovine serum (FBS) (Gibco, Rockville, MD, USA); 0.25% trypsin-EDTA solution, penicillin-streptomycin, and phosphate-buffered saline (PBS) (Hyclone, Logan, UT, USA); protein extraction kit (KEYGEN, Nanjing, China); AKT, PI3K, ERK1, IkB, IKK antibody, and GAPDH antibody (Wanleibio, Shenyang, China); CD29 antibody, CD34 antibody, and CD44 antibody (Abcam, Cambridge, MA, USA); and cell counting kit-8 (CCK-8) (Beyotime Biotechnology, Shanghai, China).

(3) Instrument. The following instruments were used for this study: $CO_2$ incubator (NuAire, MN, USA), Multiskan spectrum (BioTek Instruments, VT, USA), flow cytometer (Beckman Coulter, CA, USA), high-performance centrifuge (Eppendorf, Hamburg, German), western blot system (Tanon Science & Technology, Shanghai, China), ice machine (XUEKE ELECTRIC, Changshu, China), inverted microscope (Olympus Corporation, Tokyo, Japan), cell counter (Countstar, Shanghai, China), clean bench (AIR-TECH, Suzhou, China), cell culture plates, and cell culture flasks (Corning, NY, USA).

### 2.10.2. Isolation, Culture, and Identification of Cells.

This investigation was approved by the Ethics Committee of the Anhui University of Chinese Medicine. Written informed consent was obtained from all participants before the study. Bone marrow was obtained from OP patients who underwent surgery in the orthopedics department of the First Affiliated Hospital of Anhui University of Traditional Chinese Medicine and volunteered to participate in this study. Separating and culturing hBMSCs (human bone marrow mesenchymal stem cells) via the method of whole bone marrow adherent. Bone marrow samples applied in cell culture plates were cultured in HG-DMEM containing 10% FBS, 100 U/mL penicillin, and 100 μg/mL streptomycin, then cultured in a 37°C incubator with a 5% $CO_2$ atmosphere. The medium was changed every 2 days until the cells became confluent, about 80%–90%. The cells were then passaged. The surface marker phenotypes (CD29+, CD44+, and CD34−) were characterized by using flow cytometry.

After the cells were confirmed to be hBMSCs, cells from passages 3 to 5 were used in subsequent experiments.

### 2.10.3. Preparation and Preservation of CKG-Medicated Serum.

The experiment was approved by the Animal Ethics Committee of the Anhui University of Chinese Medicine. Twenty-four 4-week-old SPF Sprague–Dawley rats weighing 200–250 g, half male and half female, were purchased from the Experimental Animal Center of Anhui Medical University (Experimental Animal Production License Number: SCXK (Wan) 2017-001). Animals were placed in plastic cages at $22 \pm 1°C$ with a 12 h light-dark cycle. Food and water were available ad libitum. They adapted for a week in this environment. The decoction method of the CKG prescription is as follows: after 60 minutes of soaking in sufficient water, the original drugs with the water were decocted in a Chinese herbal medicine decoction machine, then brought to a boil over high heat, and then simmered for 1 hour. The process was repeated three times. The decocting solution was pooled together, added into an electrothermal constant temperature water tank, and concentrated to 2.9 g of the original drugs per mL. The samples were sealed and stored in a refrigerator at 4°C. Animals were randomly divided into medicated serum (MS) ($n = 12$) and nonmedicated serum (NS) ($n = 12$) groups. MS group animals were administered intragastrically with CKG concentrated liquor (20 mL/kg) once a day for 7 days. NS group animals were administered intragastrically saline on the same schedule. 12 h before the final treatment, fasting but not watering. 1 h after the final treatment, rats were weighed and intraperitoneally anesthetized using 1% pentobarbital sodium (60 mg/kg). Blood was collected from the abdominal aorta. The collected blood was allowed to stand at room temperature for one hour, then centrifuged at 3000 r/min for 15 min, and the upper serum was taken from the ultraclean workbench. Serum samples from all individual animals of each group were pooled. Then, it was filtered through a 0.22 $\mu$m filter membrane, heat-inactivated at 56°C for 30 min, and stored at −80°C until used.

### 2.10.4. Detect the Promoting Effect of CKG-Medicated Serum on Cell Proliferation.

Cells were collected in the logarithmic growth phase and a single cell suspension was prepared. Cells were seeded into 96-well microplates at $1 \times 10^4$ cells/well in 200 $\mu$L medium after counting with a cell counter. NS and MS (at concentrations of 2, 5, and 8%) were added to the culture medium for 24 h. The culture medium was then removed and 100 $\mu$L of CKK-8 solution was added to the well and incubated for 24 h, 36 h, and 48 h. Subsequently, the CKK-8 solution was removed, and 100 $\mu$L of DMSO was added to dissolve the formazan crystals. The optical density (OD) value was read at 450 nm by using a microplate reader. Cell proliferation rate = $(OD_{MS} - OD_{NS})/OD_{NS}$.

### 2.10.5. Western Blot.

hBMSCs were plated into 6-well plates. After 12 h, they were treated with MS (at concentrations of 0, 2, 5, and 8%). The treating time is decided by the results of 2.9.3. Total proteins were extracted from the protein extraction kit, separated using SDS-PAGE, and then transferred to polyvinylidene difluoride (PVDF) membranes, which were blocked with 5% nonfat dry milk in TBST buffer. The primary antibodies were added at proper dilution and incubated at 4°C overnight, and the secondary antibody was added and incubated for 60 min, PVDF membranes were washed with precooled PBS three times. Finally, the signals for the immunoreactive proteins were visualized by enhanced chemiluminescence reagents and then analyzed with Quantity One software. The experiment was repeated 3 times independently.

## 3. Results

### 3.1. Identification of Bioactive Components in CKG.

The screening criteria were OB ≥ 30% and DL ≥ 0.18. We got 76 bioactive ingredients via the TCMSP database, including 23 of RA, 16 of RPA, 5 of RC, 26 of HE, 3 of CPM, and 3 of CO. 65 bioactive ingredients were obtained after the removal of duplicate components. Results are detailed in Table 1. Sitosterol is the common bioactive ingredient of RA, RPA, and HE. Kaempferol is the common bioactive ingredient of RA, RPA, HE, and CPM. Mairin is the common bioactive component of RA and RPA. Quercetin is the common bioactive component of RA, HE, CPM, and RC. 22, 23-Dihydrostigmasterol is the common bioactive ingredient of RPA, HE, and RC.

### 3.2. Acquisition of Drug Targets and Construction of the "D-C-T" Network.

By searching targets of the bioactive ingredients in the TCMSP database and performing protein-gene named transformations in the UniProt database, we got 1641 targets in this study. After removing duplicate data, 250 targets were obtained. After removing the bioactive ingredients without targets, they successfully constructed the "D-C-T" network by inputting the files containing drugs, bioactive ingredients with targets, and gene targets into the Cytoscape software. The squares represent drugs, the rounds represent bioactive ingredients, and the diamonds represent various targets. There are 310 nodes and 1705 edges in the "D-C-T" network. Figure 2 shows the network.

### 3.3. Acquisition of Disease Targets, Intersection Targets, and Construction of the "C-T" Network.

By searching and integrating them in the GeneCards and CTD databases, we got 1246 OP gene targets. By taking the intersection of targets of OP with targets of CKG, we got 140 intersecting genes. Figure 3 shows the drug-disease targets Venn diagram. The "C-T" network was constructed by entering 140 intersecting genes and bioactive ingredients into Cytoscape software. There are 187 nodes and 1028 edges in the "C-T" network. Table 2 shows the degree values of the compounds in the "C-T" network. Results are as detailed in Supplementary Table 1. Figure 4 shows the network.

### 3.4. Construction, Topology of PPI Network, and Acquisition of Core Genes.

We imported the obtained intersecting genes into the STRING database to acquire the interaction relationships between them and saved the data as a file in TSV format. Figure 5 shows the PPI network diagram. We

TABLE 1: The information of the bioactive compounds of CKG.

| Abbreviation | Mol. ID | Molecule name | OB (%) | DL | Herb |
|---|---|---|---|---|---|
| COMMON1 | MOL000359 | Sitosterol | 36.91 | 0.75 | RA,RPA,HE |
| COMMON2 | MOL000422 | Kaempferol | 41.88 | 0.24 | RA,RPA,HE,CPM |
| COMMON3 | MOL000211 | Mairin | 55.38 | 0.78 | RA,RPA |
| COMMON4 | MOL000098 | Quercetin | 46.43 | 0.28 | RA,HE,RC,CPM |
| COMMON5 | MOL000358 | 22,23-Dihydrostigmasterol | 36.91 | 0.75 | RPA,HE,RC |
| CPM1 | MOL002259 | Physcion diglucoside | 41.65 | 0.63 | CPM |
| RA1 | MOL000033 | (3S,8S,9S,10R,13R,14S,17R)-10,13-dimethyl-17-[(2R,5S)-5-propan-2-yloctan-2-yl]-2,3,4,7,8,9,11,12,14,15,16,17-dodecahydro-1H-cyclopenta[a]phenanthren-3-ol | 36.23 | 0.78 | RA |
| RA2 | MOL000239 | Jaranol | 50.83 | 0.29 | RA |
| RA3 | MOL000296 | Hederagenin | 36.91 | 0.75 | RA |
| RA4 | MOL000354 | Isorhamnetin | 49.6 | 0.31 | RA |
| RA5 | MOL000371 | 3,9-di-O-methylnissolin | 53.74 | 0.48 | RA |
| RA6 | MOL000378 | 7-O-methylisomucronulatol | 74.69 | 0.3 | RA |
| RA7 | MOL000379 | 9,10-dimethoxypterocarpan-3-O-$\beta$-D-glucoside | 36.74 | 0.92 | RA |
| RA8 | MOL000380 | (6aR,11aR)-9,10-dimethoxy-6a,11a-dihydro-6H-benzofurano[3,2-c]chromen-3-ol | 64.26 | 0.42 | RA |
| RA9 | MOL000387 | Bifendate | 31.1 | 0.67 | RA |
| RA10 | MOL000392 | Formononetin | 69.67 | 0.21 | RA |
| RA11 | MOL000417 | Calycosin | 47.75 | 0.24 | RA |
| RA12 | MOL000433 | FA | 68.96 | 0.71 | RA |
| RA13 | MOL000439 | Isomucronulatol-7,2′-di-O-glucosiole | 49.28 | 0.62 | RA |
| RA14 | MOL000442 | 1,7-dihydroxy-3,9-dimethoxy pterocarpene | 39.05 | 0.48 | RA |
| RA15 | MOL002565 | Calycosin-7-O-beta-D-glucopyranoside | 41.6 | 0.81 | RA |
| RA16 | MOL009289 | (−)-Medicarpin | 49.22 | 0.34 | RA |
| RA17 | MOL000374 | 5′-hydroxyiso-muronulatol-2′,5′-di-O-glucoside | 41.72 | 0.69 | RA |
| RA18 | MOL000398 | Isoflavanone | 109.99 | 0.3 | RA |
| RA19 | MOL000438 | (3R)-3-(2-hydroxy-3,4-dimethoxyphenyl)chroman-7-ol | 67.67 | 0.26 | RA |
| RPA1 | MOL001919 | (3S,5R,8R,9R,10S,14S)-3,17-dihydroxy-4,4,8,10,14-pentamethyl-2,3,5,6,7,9-hexahydro-1H-cyclopenta[a]phenanthrene-15,16-dione | 43.56 | 0.53 | RPA |
| RPA2 | MOL001924 | Paeoniflorin | 53.87 | 0.79 | RPA |
| RPA3 | MOL000492 | (+)-Catechin | 54.83 | 0.24 | RPA |
| RPA4 | MOL001918 | Paeoniflorgenone | 87.59 | 0.37 | RPA |
| RPA5 | MOL002710 | Pyrethrin II | 48.36 | 0.35 | RPA |
| RPA6 | MOL001930 | Benzoyl paeoniflorin | 31.27 | 0.75 | RPA |
| RPA7 | MOL001921 | Lactiflorin | 49.12 | 0.8 | RPA |
| RPA8 | MOL001910 | 11alpha,12alpha-epoxy-3beta-23-dihydroxy-30-norolean-20-en-28,12beta-olide | 64.77 | 0.38 | RPA |
| RPA9 | MOL001928 | Albiflorin_qt | 66.64 | 0.33 | RPA |
| RPA10 | MOL001925 | Paeoniflorin_qt | 68.18 | 0.4 | RPA |
| RPA11 | MOL007014 | 8-debenzoylpaeonidanin | 31.74 | 0.45 | RPA |
| RPA12 | MOL007025 | Isobenzoylpaeoniflorin | 31.14 | 0.54 | RPA |
| HE1 | MOL004427 | Icariside A7 | 31.91 | 0.86 | HE |
| HE2 | MOL001792 | DFV | 32.76 | 0.18 | HE |
| HE3 | MOL003044 | Chryseriol | 35.85 | 0.27 | HE |
| HE4 | MOL000006 | Luteolin | 36.16 | 0.25 | HE |
| HE5 | MOL001771 | Poriferast-5-en-3beta-ol | 36.91 | 0.75 | HE |
| HE6 | MOL001510 | 24-epicampesterol | 37.58 | 0.71 | HE |
| HE7 | MOL003542 | 8-Isopentenyl-kaempferol | 38.04 | 0.39 | HE |
| HE8 | MOL004380 | C-homoerythrinan, 1,6-didehydro-3,15,16-trimethoxy-, (3.beta.)- | 39.14 | 0.49 | HE |
| HE9 | MOL004394 | Anhydroicaritin-3-O-alpha-L-rhamnoside | 41.58 | 0.61 | HE |
| HE10 | MOL004425 | Icariin | 41.58 | 0.61 | HE |
| HE11 | MOL001645 | Linoleyl acetate | 42.1 | 0.2 | HE |
| HE12 | MOL004373 | Anhydroicaritin | 45.41 | 0.44 | HE |
| HE13 | MOL004384 | Yinyanghuo C | 45.67 | 0.5 | HE |
| HE14 | MOL004391 | 8-(3-methylbut-2-enyl)-2-phenyl-chromone | 48.54 | 0.25 | HE |
| HE15 | MOL004386 | Yinyanghuo E | 51.63 | 0.55 | HE |
| HE16 | MOL004396 | 1,2-bis(4-hydroxy-3-methoxyphenyl)propan-1,3-diol | 52.31 | 0.22 | HE |
| HE17 | MOL004382 | Yinyanghuo A | 56.96 | 0.77 | HE |

TABLE 1: Continued.

| Abbreviation | Mol. ID | Molecule name | OB (%) | DL | Herb |
|---|---|---|---|---|---|
| HE18 | MOL004388 | 6-hydroxy-11,12-dimethoxy-2,2-dimethyl-1,8-dioxo-2,3,4,8-tetrahydro-1H-isochromeno[3,4-h]isoquinolin-2-ium | 60.64 | 0.66 | HE |
| HE19 | MOL004367 | Olivil | 62.23 | 0.41 | HE |
| HE20 | MOL000622 | Magnograndiolide | 63.71 | 0.19 | HE |
| HE21 | MOL002556 | 7-methoxy-8-(2′-hydroxy-3′-ethoxy-3′-methylbutyl)coumarin | 40.36 | 0.21 | HE |
| HE22 | MOL008046 | 6-demethoxycapillarisin | 52.33 | 0.25 | HE |
| RC1 | MOL012298 | Rubrosterone | 32.69 | 0.47 | RC |
| RC2 | MOL012286 | Betavulgarin | 68.75 | 0.39 | RC |
| RC3 | MOL012542 | $\beta$-ecdysterone | 44.23 | 0.82 | RC |
| CO1 | MOL010617 | 5,8,11,14,17-eicosapentaenoic acid | 45.66 | 0.21 | CO |
| CO2 | MOL005320 | Eicosanetetraenoic acid | 45.57 | 0.2 | CO |
| CO3 | MOL010861 | Vitamin D3 | 45.66 | 0.48 | CO |
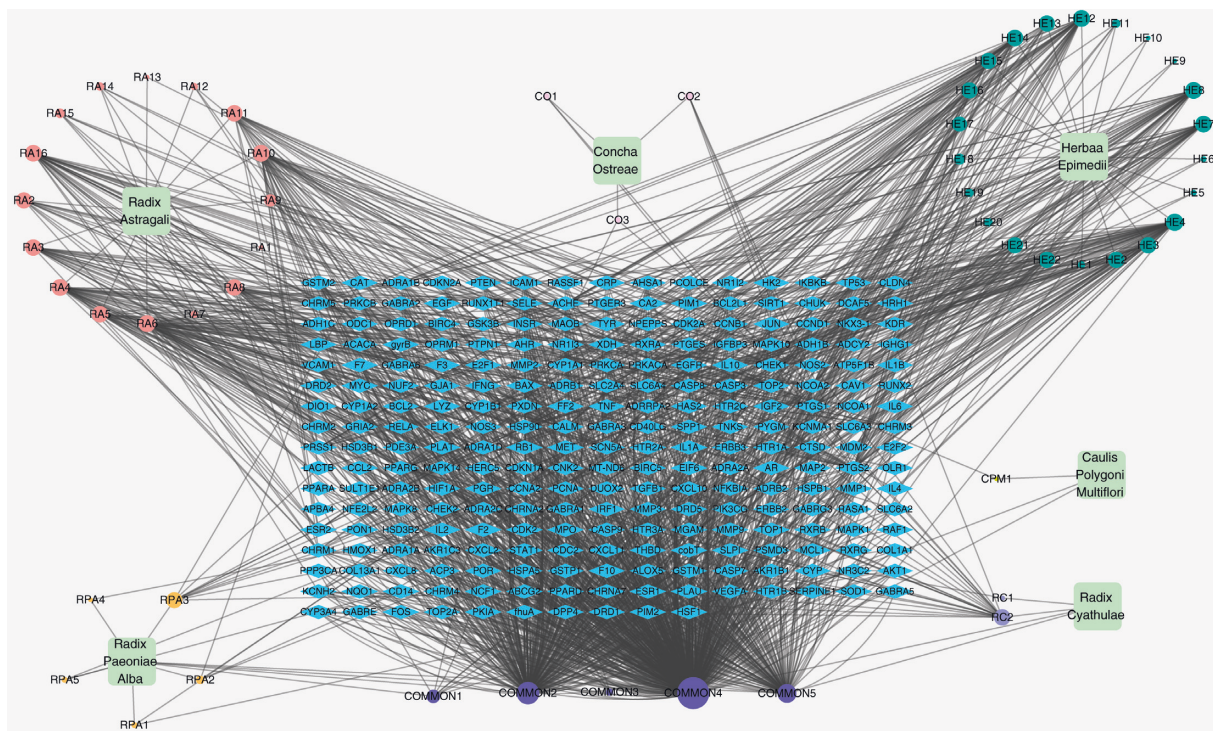


FIGURE 2: drug-compound-target network. Blue diamond nodes indicate targets, cyan square nodes indicate herbs, coral red round nodes indicate bioactive ingredients of RA, chrome yellow round nodes indicate bioactive ingredients of RPA, dark green round nodes indicate bioactive ingredients of HE, lilac round nodes indicate bioactive ingredients of CO, bright yellow round nodes indicate bioactive ingredients of CPM, lavender round nodes indicate bioactive ingredients of RC, and dark purple round nodes indicate bioactive ingredients of herbs together. The size of the compound-related nodes indicates the size of the degree value.
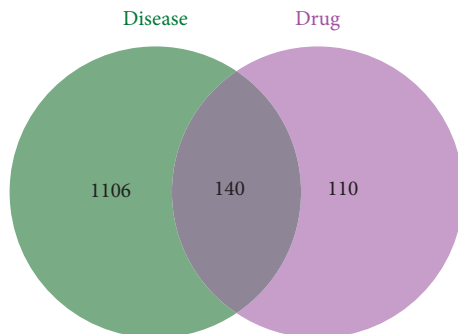


FIGURE 3: Drug-disease targets Venn diagram.

TABLE 2: The abbreviations and degree values of the top 10 bioactive ingredients of the "C-T" network.

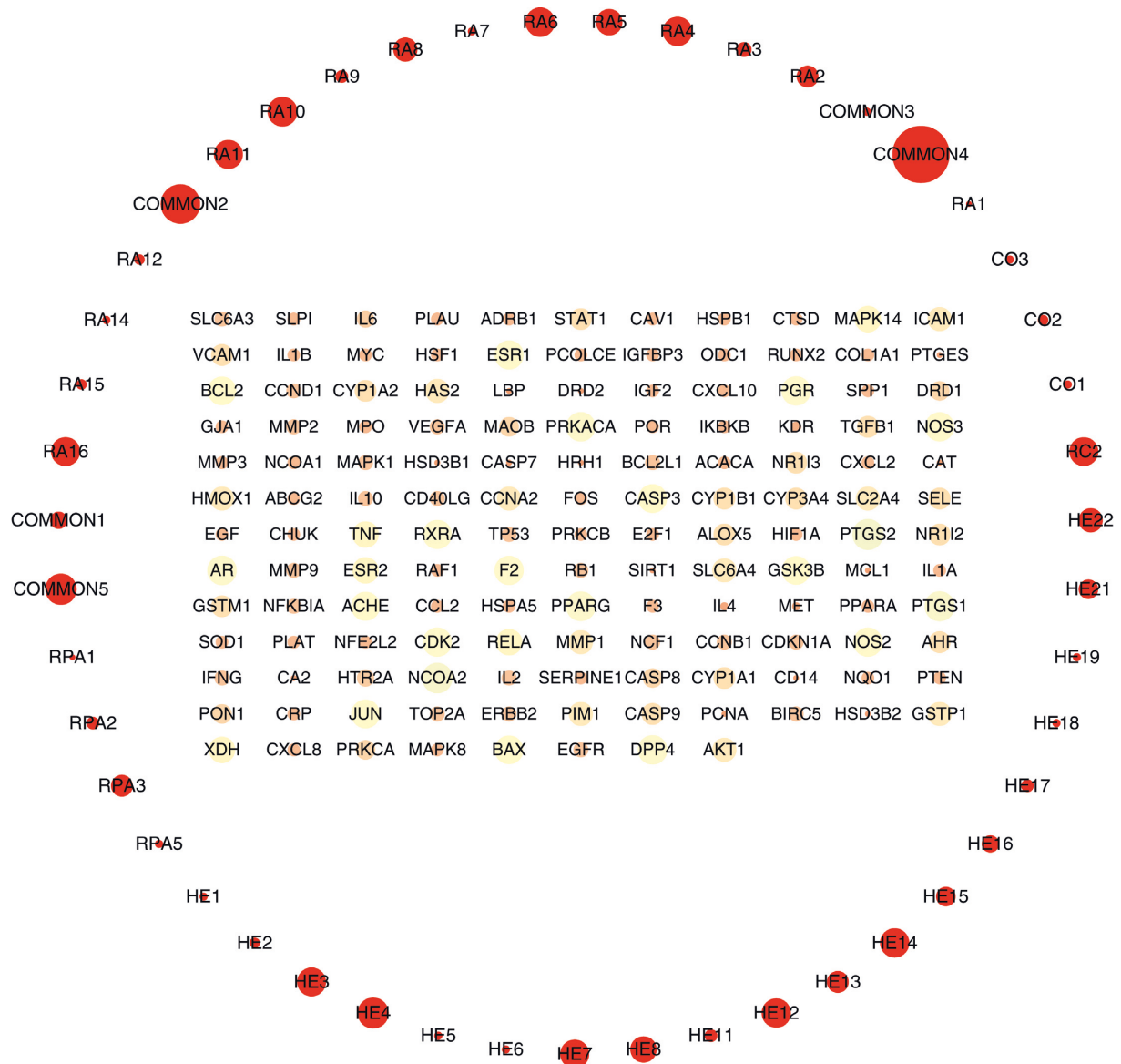| Abbreviation | Degree |
| --- | --- |
| COMMON4 | 431 |
| COMMON2 | 170 |
| COMMON5 | 51 |
| HE4 | 46 |
| RA10 | 27 |
| RA6 | 23 |
| RA4 | 22 |
| HE12 | 20 |
| HE14 | 20 |
| RA11 | 16 |



FIGURE 4: The compound-target network. The colored circular nodes indicate the intersecting gene targets, and the red circular nodes indicate the bioactive components of CKG. The size of the nodes indicates the size of the degree value.

imported the TSV data into Cytoscape software. The network has 113 nodes and 350 edges. Then they used CytoNCA to analyze the PPI network based on DC, BC, and CC parameters. The criteria for the first screening were Degree ≥4, BC ≥ 0.0055, and CC ≥ 0.324. The results showed 43 nodes and 186 edges. The second screening threshold was Degree ≥8, BC ≥ 0.0116, and CC ≥ 0.35. The second screening result was 23 nodes and 94 edges. Figure 6 shows
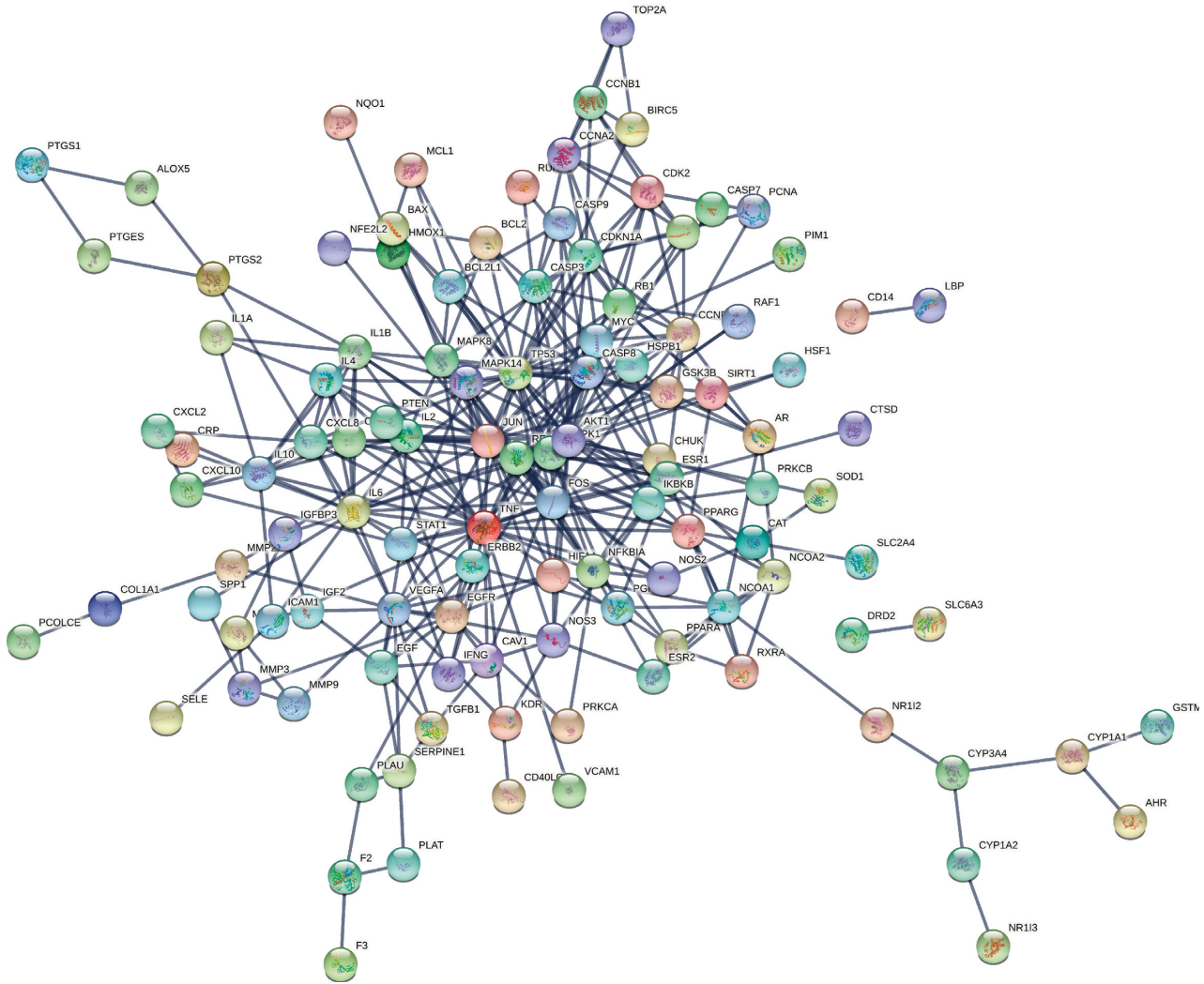
FIGURE 5: The protein-protein interaction network of targets of CKG against OP.

the process of topology. The core genes were JUN, TP53, TNF, AKT1, MAPK1, RELA, IL6, VEGFA, RB1, ESR1, CDKN1A, MYC, CCND1, CASP8, MAPK14, FOS, CXCL8, IL1B, EGFR, NFKBIA, STAT1, PPARG, and NOS3. Figure 7 shows the hub genes. Table 3 shows the top 5 degree values of hub genes.

*3.5. Enrichment Analysis of GO and KEGG.* GO enrichment analysis got 1723 entries, of which 1621 were BP entries, 20 were CC entries, and 82 were MF entries. BP analysis showed the targets principally relate to regulating DNA-binding transcription factor activity, response to lipopolysaccharide, response to molecules of bacterial origin, response to mechanical stimulus, cellular response to biotic stimulus, cellular response to lipopolysaccharide, epithelial cell proliferation, cellular response to molecules of bacterial origin, response to reactive oxygen species, and muscle cell proliferation. Analysis of the CC category showed the targets mostly within nuclear chromatin, the RNA polymerase II transcription factor complex, the transcription factor complex, the nuclear transcription factor complex, the

cyclin-dependent protein kinase holoenzyme complex, membrane raft, membrane microdomain, membrane region, the serine/threonine-protein kinase complex, the transferase complex, and the transferring phosphorus-containing groups. The MF of these proteins includes ubiquitin-like protein ligase binding, activating transcription factor binding, ubiquitin protein ligase binding, phosphatase binding, protein phosphatase binding, RNA polymerase II transcription factor binding, cytokine receptor binding, core promoter binding, DNA-binding transcription activator activity, RNA polymerase II-specific, and repressing transcription factor binding. The results of the GO analysis are as shown in Figure 8. The KEGG enrichment analysis yielded 180 entries, including the MAPK signaling pathway, the TNF signaling pathway, the PI3K-Akt signaling pathway, osteoclast differentiation, the NF-kappa B signaling pathway, and the Wnt signaling pathway. Figure 9 shows the top 20 filtered pathways most closely related to OP for the KEGG enrichment analysis. According to the KEGG analysis of the hub genes, we obtained the signal pathway diagrams of the MAPK signaling pathway, the PI3K-Akt signaling pathway, and the TNF signaling
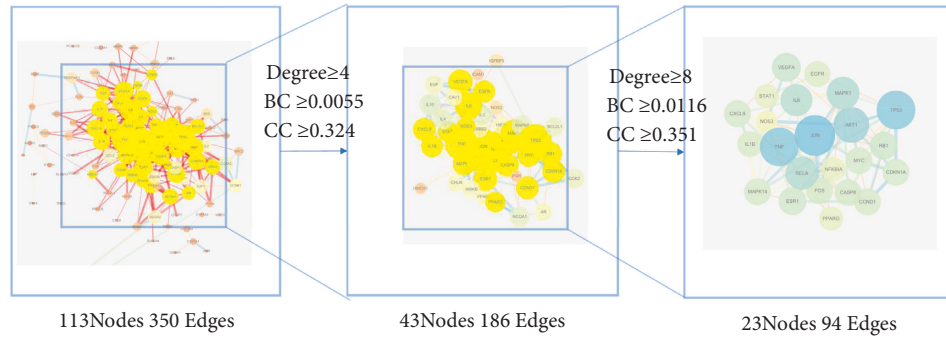
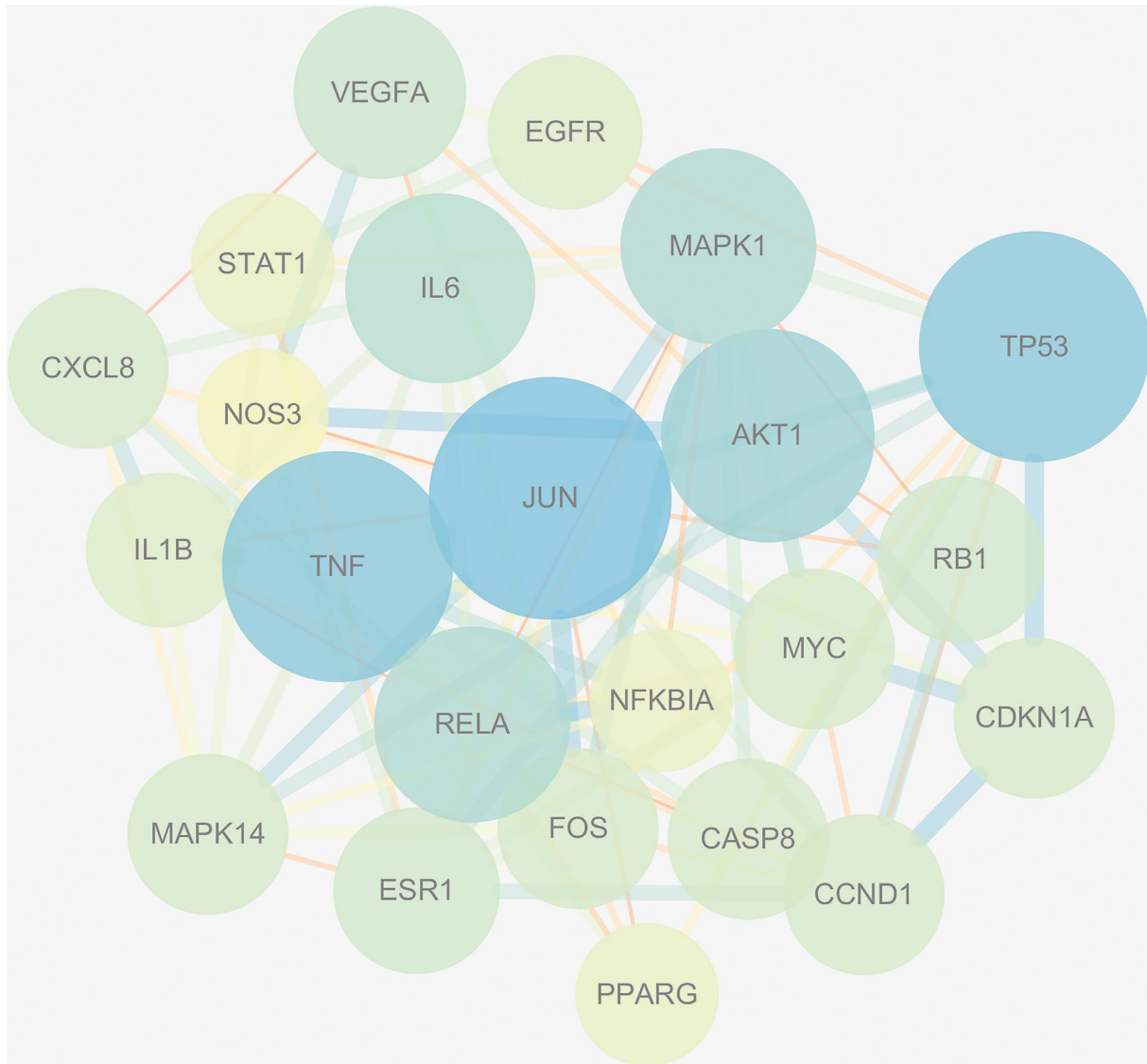FIGURE 6: The process of topological screening for the PPI network.



FIGURE 7: The network of the top 23 hub genes.

pathway. Comprehensively analyzing the three pathways, we can conclude that these pathways are all regulated by Akt, which can negatively regulate Raf, thereby affecting the Ras/MAPK signaling pathway. Akt regulates NF-kB by phosphorylating IKK and is directly involved in the regulation of the PI3K-Akt signaling pathway. The diagrams of the three signal pathways and their interconnection are stored in Supplementary Table 5.

TABLE 3: Top 5 hub genes of treating OP of CKG and topological values.

| Name | Betweenness centrality | Closeness centrality | Degree |
| --- | --- | --- | --- |
| JUN | 0.14728269 | 0.46551724 | 27 |
| TP53 | 0.1435125 | 0.43724696 | 25 |
| TNF | 0.11585625 | 0.42687747 | 25 |
| AKT1 | 0.10719742 | 0.41698842 | 22 |
| MAPK1 | 0.07457652 | 0.421875 | 19 |
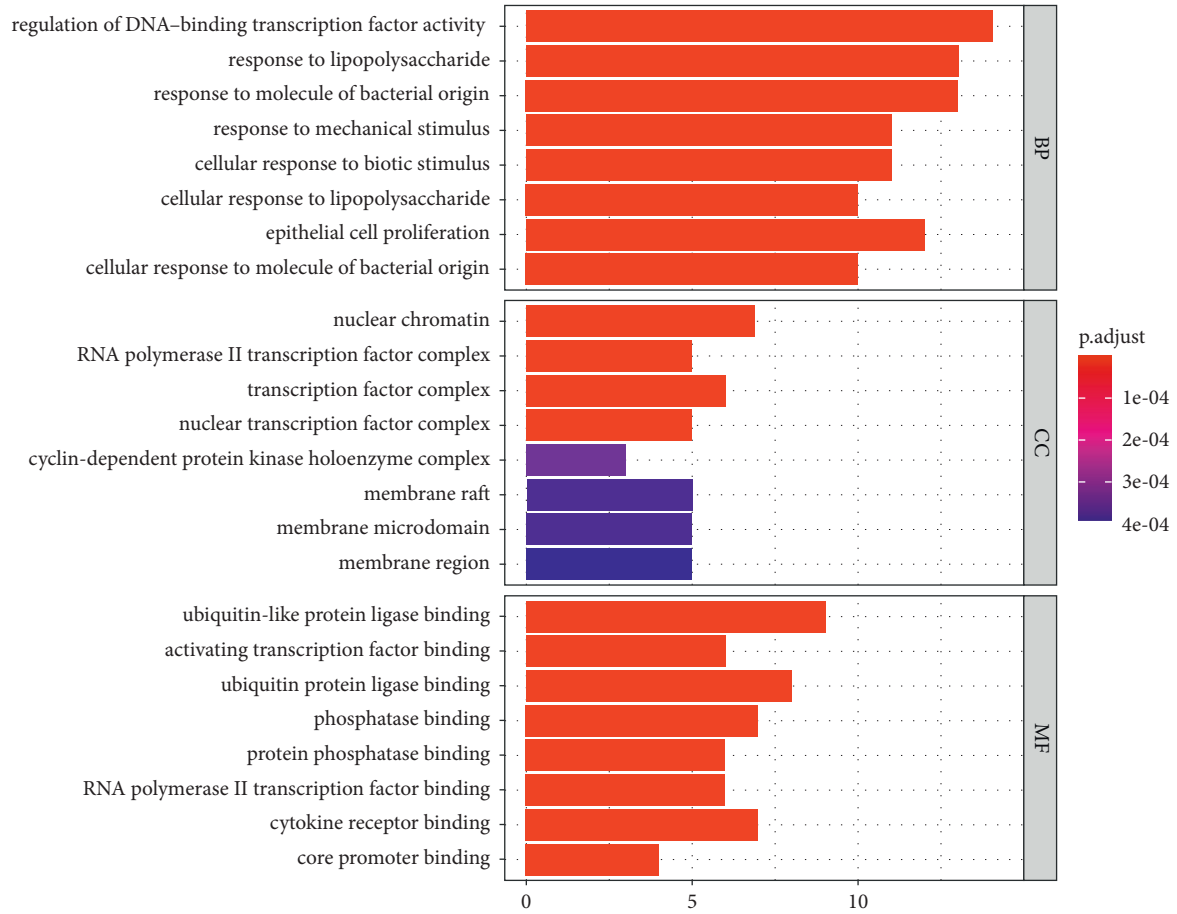


FIGURE 8: GO enrichment analysis.

*3.6. Molecular Docking Analysis.* Five core targets JUN, TNF, TP53, Akt1, and MAPK1 were selected based on the degree values, and then molecularly docked with the core bioactive ingredients kaempferol, quercetin, 22,23-dihydrostigmasterol, luteolin, anhydroicaritin, 8-(3-methylbut-2-enyl)-2-phenyl-chromone, isorhamnetin, formononetin, calycosin, and 7-O-methylisomucronulatol obtained by swiping the degree values. It is generally accepted that for a protein-ligand complex, the lower the binding energy, the higher the binding affinity. We set binding energy $\leq -5.0$ kJ/mol as the standard. Figure 10 shows the results of molecular docking. The results in Figure 10 show that the minimum binding energy of all selected bioactive ingredients to the receptor is much less than $-5.0$ kJ/mol. Table 4 shows the specific information of the lowest binding energy among the 10 active ingredients docked with each core target. Figure 11 shows the visualization of the docking results. The molecular docking results show the vital bioactive ingredients have excellent binding to the core targets for OP treatment.

*3.7. Experimental Verification*

*3.7.1. Characteristics and Identification of hBMSC Phenotypes.* All primary cell cultures were used at early passages (3–5 passage), as shown in Figures 12(a)–12(d). After 6 days of primary culture, hBMSCs had attached, exhibited spindle and flat shapes, and reached a confluence of around 70%. Passage 2 and 3 hBMSCs reached 85% confluence on day 5 after passaging. Passage 4 hBMSCs reached 85% confluence on day 4 after passaging and resembled a shoal of fish. As shown in Figures 12(e)–12(g), P4 cells were detected with flow cytometry. Notably, the cells
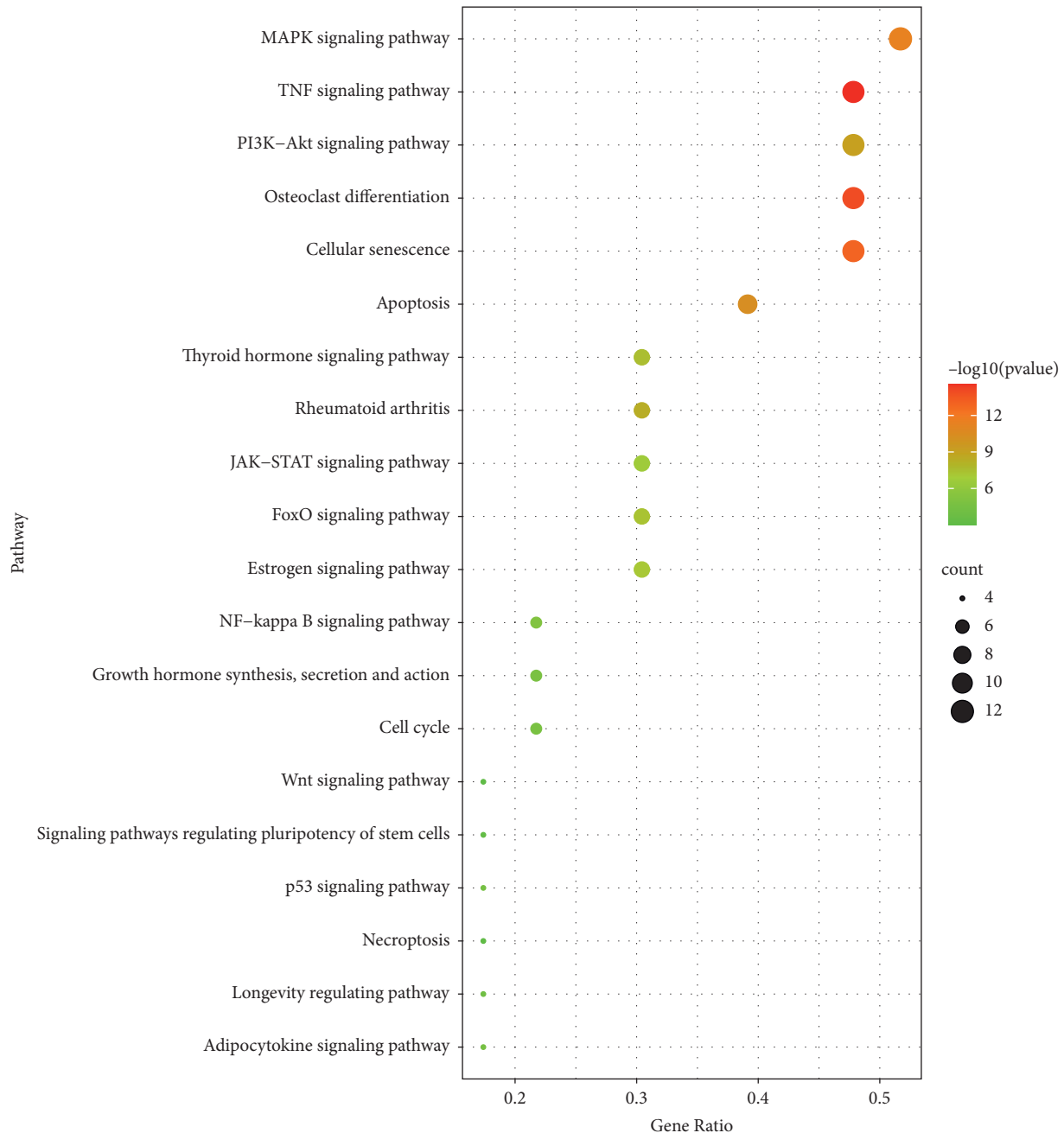
Figure 9: KEGG enrichment analysis.

were positive for the typical hBMSCs markers CD29 (98.9%) and CD44 (99%), with concomitant absence of CD34 (0.02%). Therefore, we concluded that most of the isolated and purified cells expressed standard markers of hBMSCs.

*3.7.2. The Promoting Effect of CKG-Medicated Serum on Cell Proliferation.* To detect the effect of CKG-medicated serum on hBMSCs' growth, we incubated cells in basic medium with different concentrations of NS and MS (2, 5, or 8%) for 24, 36, and 48 h. According to the results of the CCK-8 assay (Figure 13), the CKG-medicated serum treatment

significantly improved hBMSCs growth at different time points. The cell proliferation rate was the highest when cells were treated with 5% MS for 36 h ($P < 0.05$).

*3.7.3. Western Blot.* Comprehensively analyzing the screening results of the core targets and the KEGG enrichment analysis results, we can infer that CKG exerts its antiosteoporosis influence through multiple pathways. The top 3 pathways most closely related to OP in KEGG enrichment analysis are the MAPK signaling pathway, the PI3K-Akt signaling pathway, and the TNF signaling pathway. The top 5 core targets of CKG for treating OP are JUN,
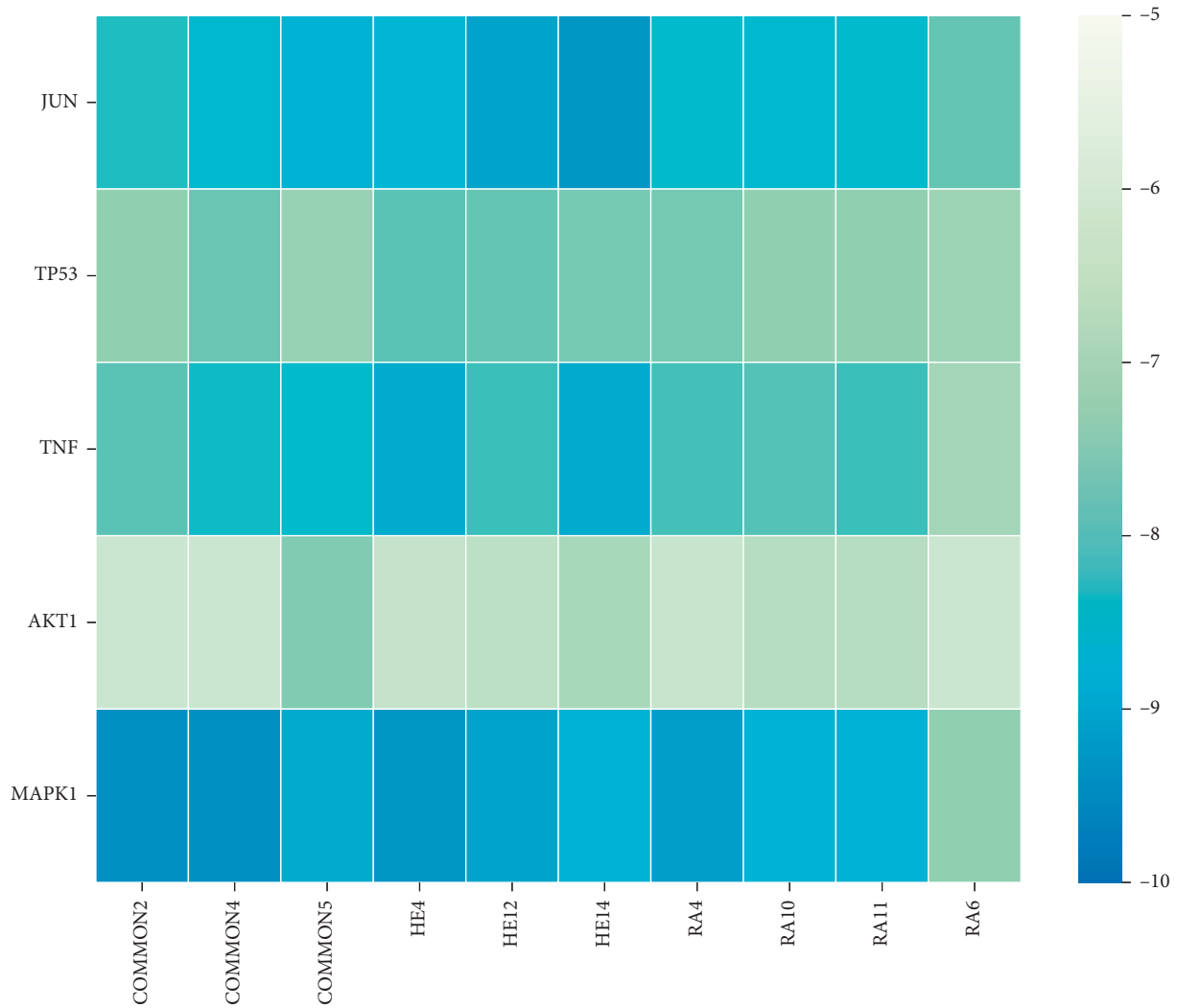
FIGURE 10: Heat maps of molecular docking between bioactive ingredients of CKG and core targets.

TABLE 4: Docking scores of the top 10 bioactive ingredients of CKG with 5 core targets.

| Target | PDB ID | Compound | Affinity (kcal/mol) |
| --- | --- | --- | --- |
| JUN | 2g01 | 8-(3-methylbut-2-enyl)-2-phenyl-chromone | −9.3 |
| TP53 | 2j21 | Luteolin | −7.8 |
| TNF | 2az5 | Luteolin | −9 |
| AKT1 | 1unq | 22,23-Dihydrostigmasterol | −7.4 |
| MAPK1 | 3w8q | Kaempferol | −9.4 |



FIGURE 11: Continued.

(e)

(f)

(g)

(h)

(i)

(j)
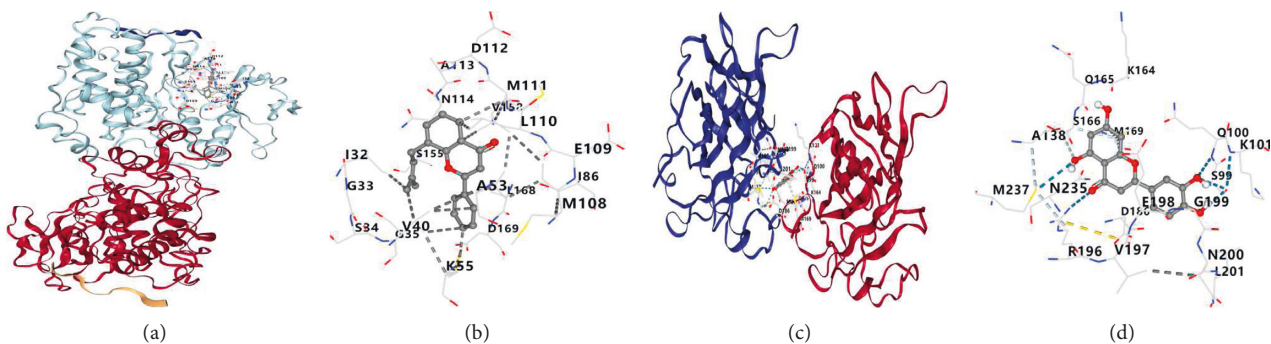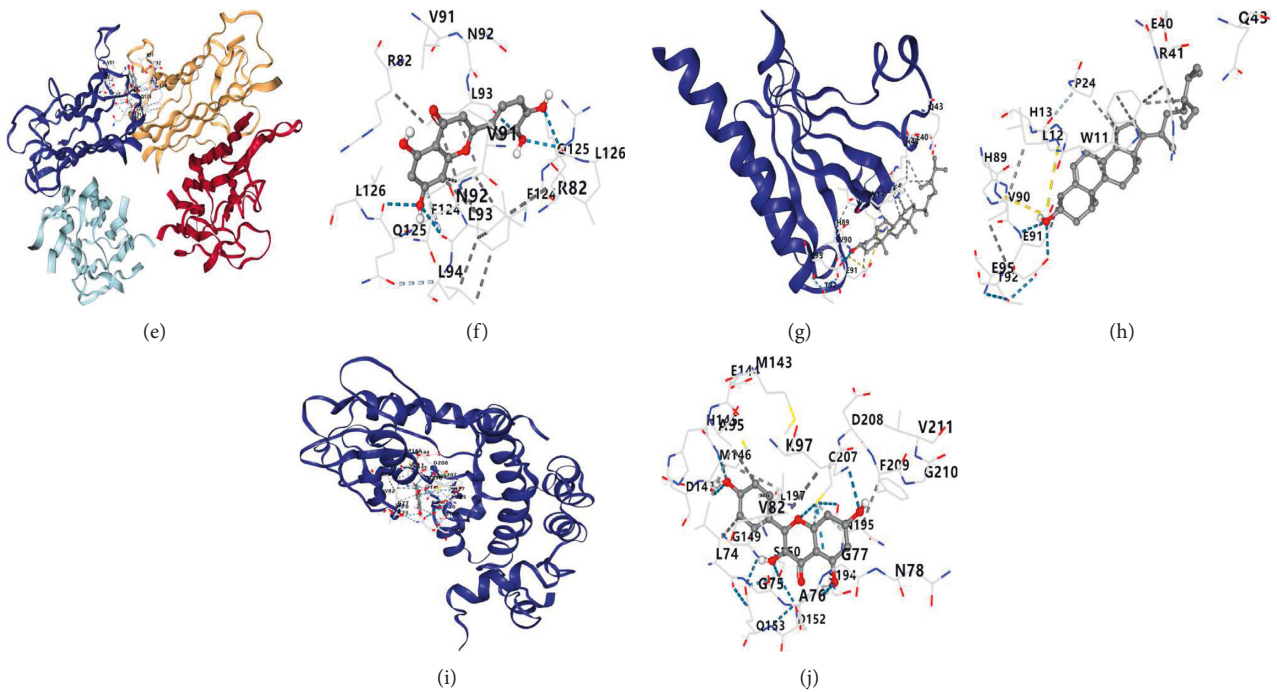
FIGURE 11: Binding mode and a 2D interaction map of compounds with core targets. (a) The binding mode of 8-(3-methylbut-2-enyl)-2-phenyl-chromone with JUN; (b) the 2D interaction map of 8-(3-methylbut-2-enyl)-2-phenyl-chromone with JUN; (c) the docking process of luteolin with TP53; (d) the 2D interaction map of luteolin with TP53; (e) the binding mode of luteolin with TNF; (f) the 2D interaction map of luteolin with TNF; (g) the binding mode of 22,23-dihydrostigmasterol with AKT1; (h) the 2D interaction map of 22,23-dihydrostigmasterol with AKT1; (i) the binding mode of kaempferol with MAPK1; and (j) the 2D interaction map of kaempferol with MAPK1.
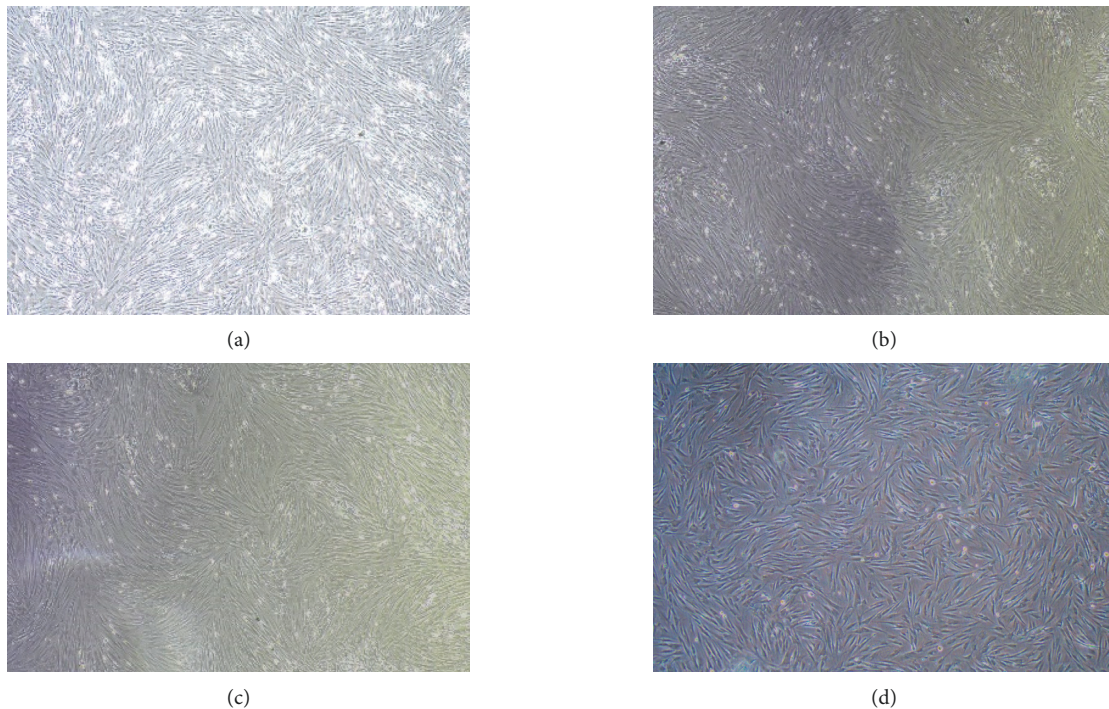


(a)
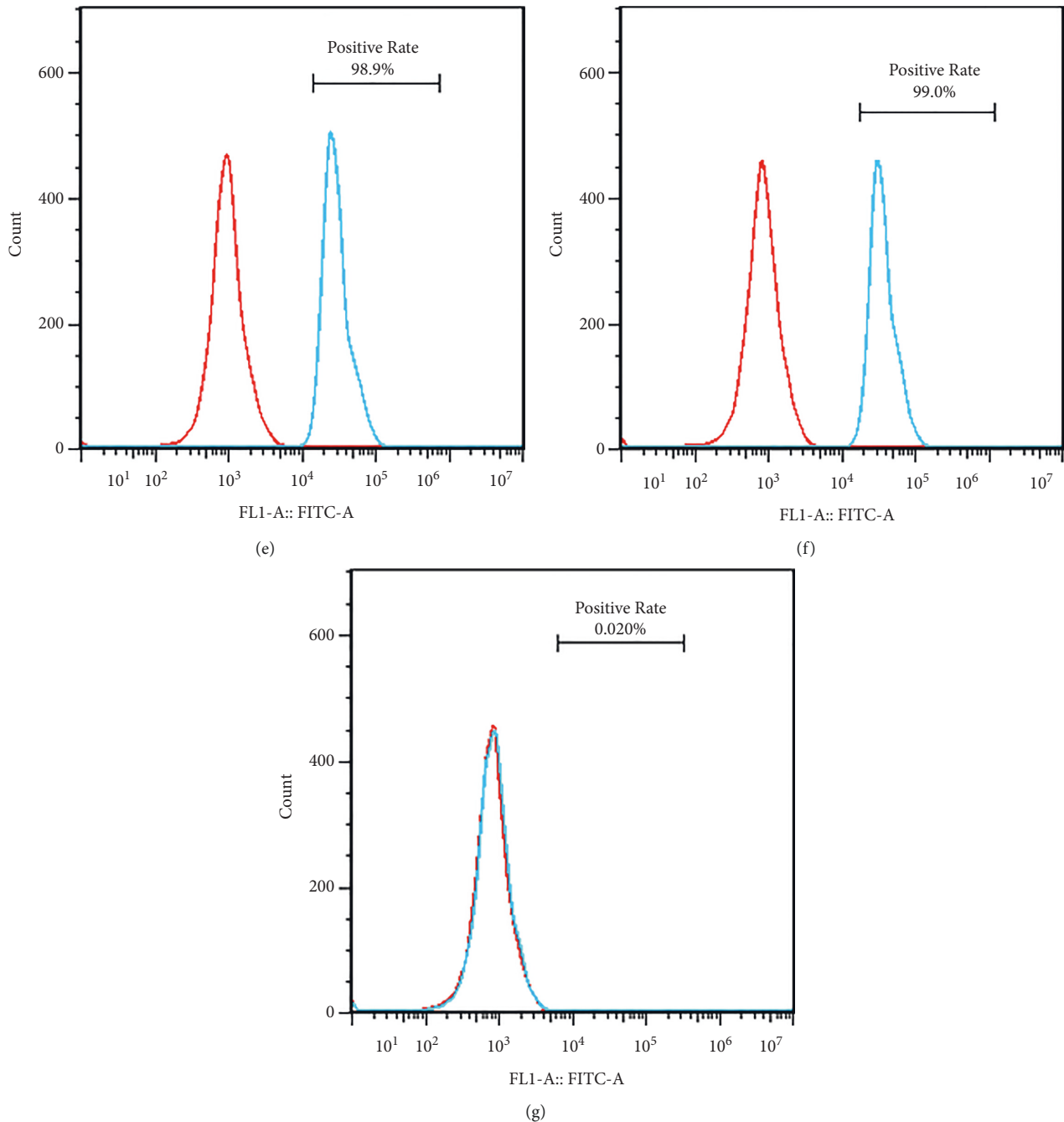
(b)

(c)

(d)

FIGURE 12: Continued.

(e)



(f)



(g)

FIGURE 12: Identification of hBMSCs. hBMSCs at passage 4 were identified with flow cytometry. (a–d) The cell morphology of passage 1 (day 6), 2 (day 5), 3 (day 5), and 4 (day 4), respectively. Flow cytometry was used to analyze the levels of the biomarkers in hBMSCs (e–g). The hBMSCs were positive for CD29 (e), CD44 (f), and negative for CD34 (g).

TNF, TP53, AKT1, and MAPK1. AKT plays an important role in the MAPK signaling pathway, the PI3K-Akt signaling pathway, and the TNF signaling pathway. AKT can negatively regulate B-Raf through phosphorylation of the B-Raf amino-terminal regulatory domain, which in turn affects the Ras/Raf pathway [28]. The inhibition of AKT leads to the enhancement of Ras/MAPK signaling [29]. TNF-$\alpha$ up-regulates several molecules such as the P2X7 receptor through the PI3K-Akt signaling pathway, the intracellular calcium concentration and secondary messengers, the entry of transcription factors into the nucleus, and the differentiation of bone marrow mesenchymal stem cells into osteoclasts [30]. Therefore, this study chose to observe the effect of CKG-medicated serum on the MAPK, PI3K-Akt, and TNF pathway-associated proteins in hBMSCs to verify that CKG participates in the MAPK signaling pathway, the PI3K-Akt signaling pathway, and the TNF signaling pathway by regulating AKT to play its part in treating OP.

Western blot results are shown in Figure 14. The histograms show quantitation of MAPK, PI3K-Akt, and TNF
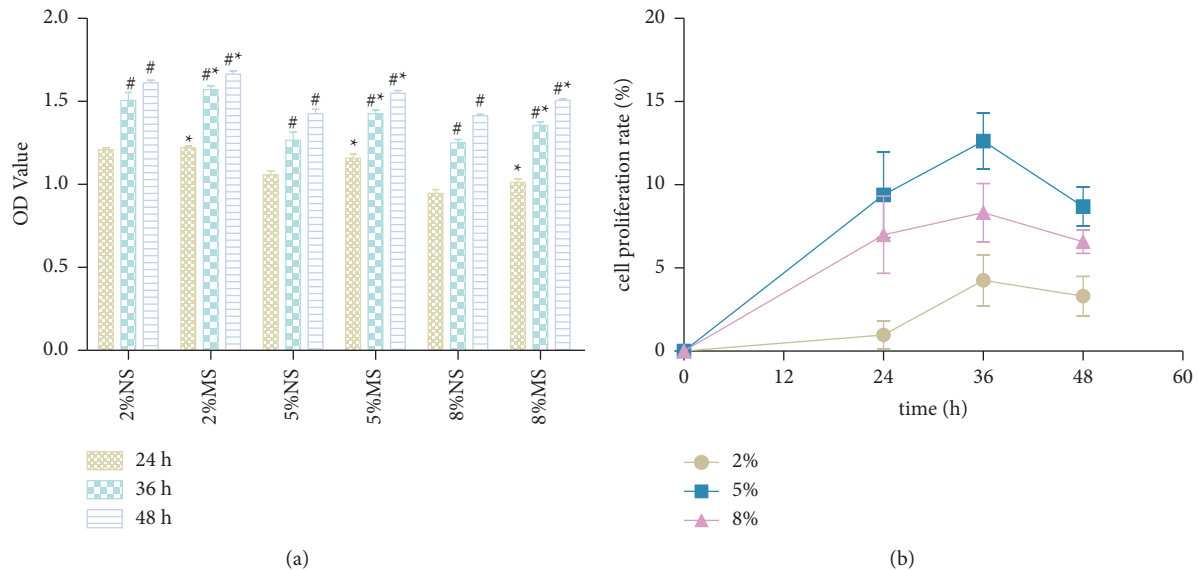
FIGURE 13: CKG-medicated serum treatment increased the proliferation of hBMSCs. (a) The CKG-medicated serum treatment for 24, 36, and 48 h significantly increased the proliferation of hBMSCs ($n = 6$). $^* P < 0.05$, compared to the NS group of the same concentration; $^\# P < 0.05$, compared to the last treatment time. (b) CKG-medicated serum increase hBMSCs proliferation rate, especially when treated with 5% MS for 36 h.

pathway-associated proteins in hBMSCs. Compared with NS, after 36 h of treatment, the AKT, PI3K, ERK1, and IkB protein expression levels in hBMSCs treated with 2, 5, and 8% MS increased. The gradual increase of AKT, PI3K, ERK1, and IkB protein expression levels was detected prominently by western blot as the CKG-MS concentration gradually increased. Compared with NS, after 36 h of treatment, the IKK protein expression levels in hBMSCs treated with 2, 5, and 8% MS decreased. The gradual decrease of IKK protein expression levels was detected prominently by western blot as the CKG-MS concentration gradually increased.

## 4. Discussion

OP is a metabolic disease caused by various factors, such as age, endocrine, viral infection, and various cytokines [31–33]. Given the multitarget and multipathway pharmacological properties of TCM, we think it is more effective in the treatment of OP. This characteristic of TCM may make it difficult to further study its intrinsic mechanisms. A network pharmacology approach combining systems biology and computer technology may provide a direction for the study of the complex mechanism of TCM [11]. In the present study, we used this approach to clarify the pharmacological mechanisms of OP alleviation by CKG.

In summary, this study analyzed the application of CKG in OP treatment by network pharmacology. We got 69 chemical ingredients, 250 targets of CKG, 1246 disease targets of OP, and 140 intersecting targets of CKG and OP. Topological analysis of the PPI network yielded 23 hub genes. GO enrichment analysis got 1723 entries, of which 1621 were BP entries, 20 were CC entries, and 82 were MF entries. The KEGG enrichment analysis yielded 180 entries. According to enrichment analysis and molecular docking

technique, we inferred that the compounds of CKG (kaempferol, quercetin, 22,23-dihydrostigmasterol, luteolin, anhydroicaritin, 8-(3-methylbut-2-enyl)-2-phenyl-chromone, isorhamnetin, formononetin, calycosin, and 7-O-methylisomucronulatol) could exert antiosteoporosis effects by targeting multiple proteins (JUN, TNF, TP53, AKT1, and MAPK1) and signaling pathways (TNF signaling pathway, osteoclast differentiation, MAPK signaling pathway, PI3K-Akt signaling pathway, NF-kappa B signaling pathway, and Wnt signaling pathway).

The three bioactive compounds in CKG with the highest degree values were 22,23-dihydrostigmasterol, kaempferol, and quercetin, which were obtained from collections of multidatabase information and stringent screening conditions. According to relevant studies, 22,23-dihydrostigmasterol (beta-sitosterol) can play an important role in antiosteoporosis treatment by affecting osteoblasts' activity [34]. Kaempferol promotes bone formation in part via the mTOR signaling pathway [35]. Quercetin inhibits osteoblast apoptosis and inflammatory response, promotes osteogenesis, angiogenesis, and osteoclast apoptosis [36]. The top five core targets in order of degree value are JUN, TNF, TP53, AKT1, and MAPK1. Based on existing relevant literature and studies, JUN accelerates the growth and healing of bone in a drilled defect model [37]. TNF-$\alpha$ directly improves RANKL expression in osteoblasts and promotes osteoclast formation [38]. Related *in vivo* and *in vitro* experiments indicated that TP53 gene expression and serum P53 levels were upregulated in OP patients and OP mouse models; high p53 levels were associated with reduced bone mass, which could be partially reversed by knocking down p53 [39]. Restraint of AKTl can inhibit BMSC proliferation driven by HB-EGF [40]. MiR-186-5p can reduce IL-1$\beta$-induced inflammatory damage of chondrocytes by
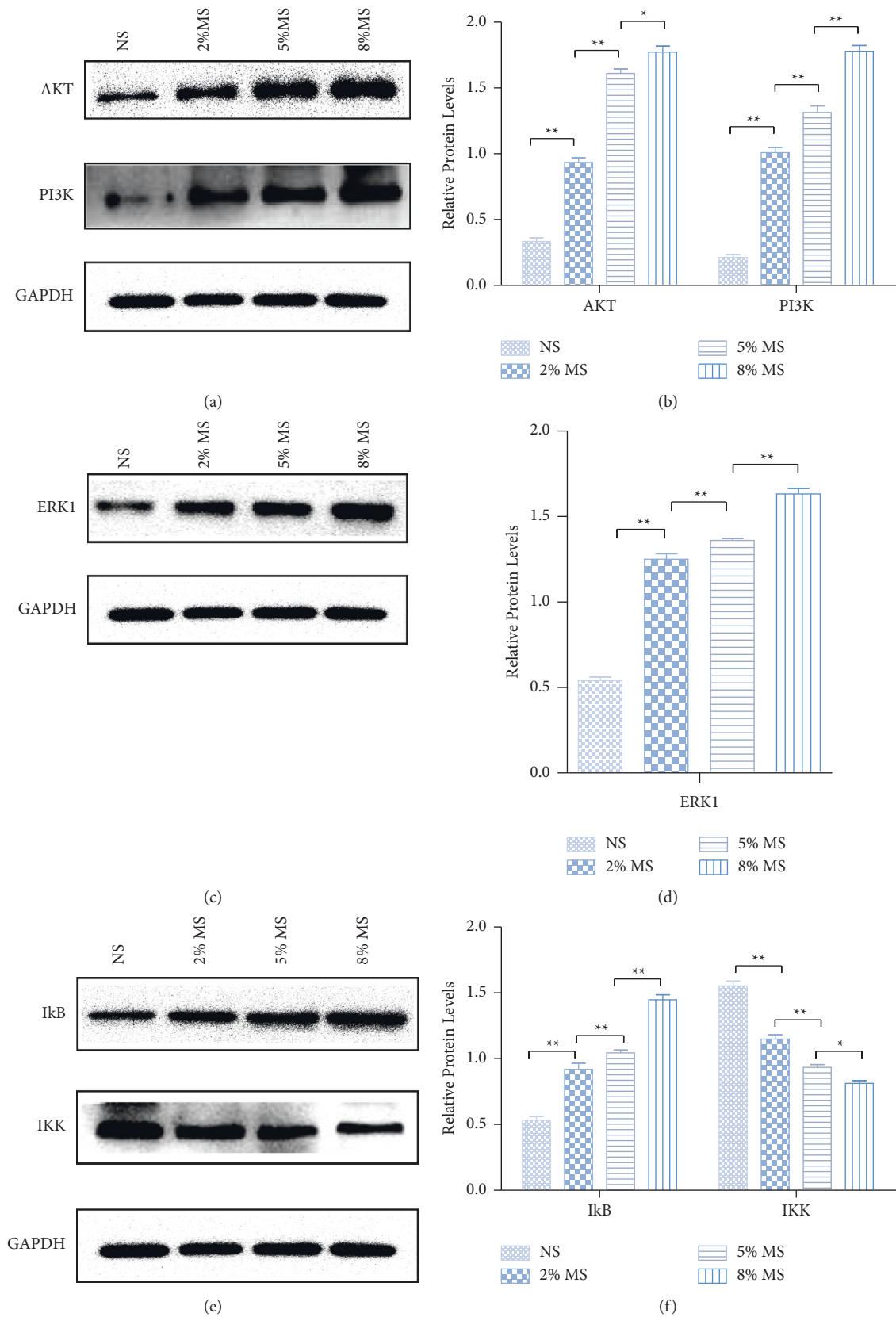
(a)

(b)

(c)

(d)

(e)

(f)

FIGURE 14: Effects of CKG-medicated serum on the expression of MAPK, PI3K-Akt, and TNF pathway-associated proteins. (a, c, e) Western blot was performed to detect AKT, PI3K, ERK1, IkB, and IKK expression levels in CKG-medicated serum-treated hBMSCs. (b, d, f) Quantification of the pathway-related proteins expression. (b) Quantification of the AKT and PI3K expression shown in (a) by normalizing to GAPDH. (d) Quantification of the ERK1 expression shown in C by normalizing to GAPDH. (f) Quantification of the IkB and IKK expression shown in (e) by normalizing to GAPDH. $*P < 0.05$ compared to the previous level group; $**P < 0.01$, compared to the previous level group.

increasing MAPK1 [41]. Enrichment analysis results showed the primary pathways in the therapeutic process include viral-related signaling pathways, bacteria-related signaling pathways, IL-17 signaling pathway, TNF signaling pathway, osteoclast differentiation, MAPK signaling pathway, PI3K-Akt signaling pathway, NF-kappa B signaling pathway, and Wnt signaling pathway. The top 3 pathways most closely related to OP in KEGG enrichment analysis are the MAPK signaling pathway, the PI3K-Akt signaling pathway, and the TNF signaling pathway. PTH induces bone loss through the microbe-dependent expansion of intestinal TNF$^+$ T cells and Th17 cells [42]. Inhibition of NF-kappa B and MAPK signaling can reduce RANKL-induced osteoclastogenesis [43]. The PI3K-Akt signaling pathway involves OP inhibition by promoting osteoblast proliferation, differentiation, and bone formation [44].

The results of molecular docking showed the core bioactive ingredients in CKG had good binding activity to the core targets for treating OP. Comprehensively analyzing the results of PPI, KEGG enrichment analysis, and molecular docking, we speculated that CKG contributes to OP treatment by engaging in multiple pathways. Analyzing the results of KEGG, we concluded that the three most important pathways are the MAPK signaling pathway, the PI3K-Akt signaling pathway, and the TNF signaling pathway. Through comprehensive analysis of the three pathways, we noticed that these pathways are all regulated by AKT, which can negatively regulate Raf, thereby affecting the MAPK signal pathway. AKT regulates the TNF pathway by phosphorylating IKK and is directly involved in the formation of the PI3K-Akt signal pathway. AKT is not only the core target screened by PPI but also the bridging protein between the top 3 pathways in the KEGG enrichment analysis. And related research studies have verified that regulating the AKT protein can affect these three pathways. Therefore, we speculate that CKG exerts an antiosteoporotic effect by affecting the expression of AKT. Then, we conducted related experiments. We used the CCK-8 method to observe the changes in cell proliferation rates after treating them with CKG-containing serum at different concentrations. Western blot was used to observe the changes of MAPK, PI3K-Akt, and TNF pathway-associated protein expression in cells treated with different concentrations of CKG-containing serum. The experimental results showed that CKG-containing serum can promote the proliferation of hBMSCs and that different concentrations of CKG-containing serum can increase the expression of AKT protein in hBMSCs. Therefore, we conclude that the antiosteoporosis effect of CKG may be achieved by regulating AKT and then engaging in the MAPK signaling pathway, the PI3K-Akt signaling pathway, and the TNF signaling pathway.

This study also has some limits, such as the accuracy and timeliness of database data, algorithms, and software characteristics of various analysis platforms. However, based on the completed research, the platforms and algorithms used in this study can meet the research needs. Besides, this study verified the mechanism of CKG in the OP treatment only through molecular docking and animal, cell, and protein experiments. But the results of this study can already

indicate that CKG is involved in the main pathway of antiosteoporosis. Thus, we need to improve related experiments later to support the theory.

## 5. Conclusion

In this study, the method of combining network pharmacology and experimental confirmation was used to investigate the complexity of multicomponent, multitarget, and multipathway of CKG, which provides essential information for further understanding of the drug-target interaction, a basis for extracting practical drug ingredients from CKG for OP treatment, and a reference for future demonstration of the scientific truth of TCM.

## Data Availability

The data used to support the findings of this study are included within the article.

## Disclosure

Hao Lv is the first author.

## Conflicts of Interest

The authors declare that they have no conflicts of interest.

## Authors' Contributions

H. Lv designed the study, analyzed the data, and wrote the manuscript. JX. Wang and YJ. Zhu analyzed the data. T. Jiang revised the manuscript. All the authors read and approved the final manuscript.

## Acknowledgments

## Supplementary Materials

Supplementary Table 1: the abbreviations and degree values of bioactive ingredients of the "C-T" network. Supplementary Table 2: hub genes of treating OP of CKG. Supplementary Table 3: the results of GO enrichment analysis. Supplementary Table 4: the KEGG enrichment analysis results of the top 20 pathways with high correlation with OP. Supplementary File 5: the diagrams of the MAPK signaling pathway, PI3K-Akt signaling pathway, TNF signaling pathway, and the relationship diagram between them. Supplementary Table 6: docking scores of the top 10 bioactive ingredients of CKG with 5 core targets. Supplementary Table 7: the result of CCK-8. Supplementary Table 8: the results of KEGG enrichment analysis. (*Supplementary Materials*)

# References

[1] B. J. Edwards, "Osteoporosis risk calculators," *Journal of Clinical Densitometry*, vol. 20, no. 3, pp. 379–388, 2017.

[2] D. L. Sietsema, "Fighting the epidemic," *Nursing Clinics of North America*, vol. 55, no. 2, pp. 193–202, 2020.

[3] Q. Zeng, N. Li, Q. Wang et al., "The prevalence of osteoporosis in China, a nationwide, multicenter DXA survey," *Journal of Bone and Mineral Research*, vol. 34, no. 10, pp. 1789–1797, 2019.

[4] S. Khosla and L. C. Hofbauer, "Osteoporosis treatment: recent developments and ongoing challenges," *Lancet Diabetes & Endocrinology*, vol. 5, no. 11, pp. 898–907, 2017.

[5] Z. Malihi, Z. Wu, A. W. Stewart, C. M. Lawes, and R. Scragg, "Hypercalcemia, hypercalciuria, and kidney stones in long-term studies of vitamin D supplementation: a systematic review and meta-analysis," *The American Journal of Clinical Nutrition*, vol. 104, no. 4, pp. 1039–1051, 2016.

[6] M. Zhou, Y. Zheng, J. Li et al., "Upper gastrointestinal safety and tolerability of oral alendronate: a meta-analysis," *Experimental and Therapeutic Medicine*, vol. 11, no. 1, pp. 289–296, 2016.

[7] Y. Takeuchi, E. Hamaya, M. Taketsuna, and H. Sowa, "Safety of 3-year raloxifene treatment in Japanese postmenopausal women aged 75 years or older with osteoporosis: a post-marketing surveillance study," *Menopause*, vol. 22, no. 10, pp. 1134–7, 2015.

[8] J. D. Zhao, Y. Q. Shu, J. Liu et al., "Clinical observation on the effect of compound kidney-invigorating granule on visual analog scale and bone mineral density in postmenopausal non-senile osteoporosis patients with kidney deficiency and blood stasis syndrome," *Chinese Journal of Osteoporosis*, vol. 24, no. 1, pp. 98–101, 2018.

[9] P. Xiao-Cong, K. De, F. Jian-Song et al., "Network pharmacology-based analysis of Chinese herbal Naodesheng formula for application to Alzheimer's disease," *Chinese Journal of Natural Medicines*, vol. 16, no. 1, pp. 53–62, 2018.

[10] J. F. Liu, A. N. Hu, J. F. Zan, P. Wang, Q. Y. You, and A. H. Tan, "Network pharmacology deciphering mechanisms of volatiles of wendan granule for the treatment of alzheimer's disease," *Evidence-based Complementary and Alternative Medicine : eCAM*, vol. 2019, Article ID 7826769, 12 pages, 2019.

[11] W. Guo, J. Huang, N. Wang et al., "Integrating network pharmacology and pharmacological evaluation for deciphering the action mechanism of herbal formula zuojin pill in suppressing hepatocellular carcinoma," *Frontiers in Pharmacology*, vol. 10, Article ID 1185, 2019.

[12] T.-T. Luo, Y. Lu, S.-K. Yan, X. Xiao, X.-L. Rong, and J. Guo, "Network pharmacology in research of Chinese medicine formula: methodology, application and prospective," *Chinese Journal of Integrative Medicine*, vol. 26, no. 1, pp. 72–80, 2020.

[13] Y. Chen, T. S. Kern, P. D. Kiser, and K. Palczewski, "Eyes on systems pharmacology," *Pharmacological Research*, vol. 114, pp. 39–41, 2016.

[14] Y. Qu, Z. Zhang, Y. Lu, D. Zheng, and Y Wei, "Network pharmacology reveals the molecular mechanism of cuyuxunxi prescription in promoting wound healing in patients with anal fistula," *Evidence-based Complementary and Alternative Medicine: ECAM*, vol. 2019, Article ID 3865121, 9 pages, 2019.

[15] J. Ru, P. Li, J. Wang et al., "TCMSP: a database of systems pharmacology for drug discovery from herbal medicines," *Journal of Cheminformatics*, vol. 6, Article ID 13, 2014.

[16] B. Li, C. Ma, X. Zhao et al., "YaTCM: yet another traditional Chinese medicine database for drug discovery," *Computational and Structural Biotechnology Journal*, vol. 16, pp. 600–610, 2018.

[17] X. Xu, W. Zhang, C. Huang et al., "A novel chemometric method for the prediction of human oral bioavailability," *International Journal of Molecular Sciences*, vol. 13, no. 6, pp. 6964–6982, 2012.

[18] W. Tao, X. Xu, X. Wang et al., "Network pharmacology-based prediction of the active ingredients and potential targets of Chinese herbal radix curcumae formula for application to cardiovascular disease," *Journal of Ethnopharmacology*, vol. 145, no. 1, pp. 1–10, 2013.

[19] C. UniProt, "UniProt: a worldwide hub of protein knowledge," *Nucleic Acids Research*, vol. 47, no. D1, pp. D506–D515, 2019.

[20] P. Shannon, A. Markiel, O. Ozier et al., "Cytoscape: a software environment for integrated models of biomolecular interaction networks," *Genome Research*, vol. 13, no. 11, pp. 2498–2504, 2003.

[21] G. Stelzer, N. Rosen, I. Plaschkes et al., "The GeneCards suite: from gene data mining to disease genome sequence analyses," *Current protocols in bioinformatics*, vol. 54, pp. 1–33, 2016.

[22] A. P. Davis, C. J. Grondin, R. J. Johnson et al., "Comparative toxicogenomics database (CTD): update 2021," *Nucleic Acids Research*, vol. 49, no. D1, pp. D1138–D1143, 2021.

[23] P. Bardou, J. Mariette, F. Escudié, C. Djemiel, and C. Klopp, "Jvenn: an interactive venn diagram viewer," *BMC Bioinformatics*, vol. 15, Article ID 293, 2014.

[24] C. V. Mering, M. Huynen, D. Jaeggi, S. Schmidt, P. Bork, and B. Snel, "STRING: a database of predicted functional associations between proteins," *Nucleic Acids Research*, vol. 31, no. 1, pp. 258–261, 2003.

[25] Y. Tang, M. Li, J. Wang, Y. Pan, and F.-X. Wu, "CytoNCA: a cytoscape plugin for centrality analysis and evaluation of protein interaction networks," *Biosystems*, vol. 127, pp. 67–72, 2015.

[26] S. Kim, J. Chen, T. Cheng et al., "PubChem in 2021: new data content and improved web interfaces," *Nucleic Acids Research*, vol. 49, no. 1, pp. D1388–D1395, 2021.

[27] S. K. Burley, H. M. Berman, C. Christie et al., "RCSB protein data bank: sustaining a living digital data resource that enables breakthroughs in scientific research and biomedical education," *Protein Science*, vol. 27, no. 1, pp. 316–330, 2018.

[28] K.-L. Guan, C. Figueroa, T. R. Brtva et al., "Negative regulation of the serine/threonine kinase B-Raf by Akt," *Journal of Biological Chemistry*, vol. 275, no. 35, pp. 27354–27359, 2000.

[29] B. Y. Shorning, M. S. Dass, M. J. Smalley, and H. B Pearson, "The PI3K-AKT-mTOR pathway and prostate cancer: at the crossroads of AR, MAPK, and WNT signaling," *International Journal of Molecular Sciences*, vol. 21, no. 12, 2020.

[30] J. Lu, Z. Zhou, J. Ma et al., "Tumour necrosis factor-α promotes BMHSC differentiation by increasing P2X7 receptor in oestrogen-deficient osteoporosis," *Journal of Cellular and Molecular Medicine*, vol. 24, no. 24, pp. 14316–14324, 2020.

[31] K. E. Ensrud and C. J. Crandall, "Osteoporosis," *Annals of Internal Medicine*, vol. 167, no. 3, pp. ITC17–ITC32, 2017.

[32] V. Pavone, G. Testa, S. M. C. Giardina, A. Vescio, D. A. Restivo, and G. Sessa, "Pharmacological therapy of osteoporosis: a systematic current review of literature," *Frontiers in Pharmacology*, vol. 8, Article ID 803, 2017.

[33] M. N. Weitzmann, "Bone and the immune system," *Toxicologic Pathology*, vol. 45, no. 7, pp. 911–924, 2017.

[34] S. Chauhan, A. Sharma, N. K. Upadhyay, G. Singh, U. Ranjan Lal, and R. Goyal, "In-vitro osteoblast proliferation and in-vivo anti-osteoporotic activity of Bombax ceiba with quantification of Lupeol, gallic acid and beta-sitosterol by HPTLC and HPLC," *BMC Complementary and Alternative Medicine*, vol. 18, no. 1, Article ID 233, 2018.

[35] J. Zhao, J. Wu, B. Xu et al., "Kaempferol promotes bone formation in part via the mTOR signaling pathway," *Molecular Medicine Reports*, vol. 20, no. 6, pp. 5197–5207, 2019.

[36] S. K. Wong, K. Y. Chin, and S. Ima-Nirwana, "Quercetin as an agent for protecting the bone: a review of the current evidence," *International Journal of Molecular Sciences*, vol. 21, no. 17, 2020.

[37] T. Lerbs, L. Cui, C. Muscat et al., "Expansion of bone precursors through jun as a novel treatment for osteoporosis-associated fractures," *Stem Cell Reports*, vol. 14, no. 4, pp. 603–613, 2020.

[38] H. Kitaura, A. Marahleh, F. Ohori et al., "Osteocyte-related cytokines regulate osteoclast formation and bone resorption," *International Journal of Molecular Sciences*, vol. 21, no. 14, 2020.

[39] T. Yu, X. You, H. Zhou et al., "p53 plays a central role in the development of osteoporosis," *Aging*, vol. 12, no. 11, pp. 10473–10487, 2020.

[40] P. Li, Q. Deng, J. Liu et al., "Roles for HB-EGF in mesenchymal stromal cell proliferation and differentiation during skeletal growth," *Journal of Bone and Mineral Research*, vol. 34, no. 2, pp. 295–309, 2019.

[41] Q. Li, M. Wu, G. Fang et al., "MicroRNA1865p downregulation inhibits osteoarthritis development by targeting MAPK1," *Molecular Medicine Reports*, vol. 23, no. 4, 2021.

[42] M. Yu, A. Malik Tyagi, J.-Y. Li et al., "PTH induces bone loss via microbial-dependent expansion of intestinal TNF$^+$ T cells and Th17 cells," *Nature Communications*, vol. 11, no. 1, Article ID 468, 2020.

[43] D. Thummuri, L. Guntuku, V. S. Challa, R. N. Ramavat, and V. G. M. Naidu, "Abietic acid attenuates RANKL induced osteoclastogenesis and inflammation associated osteolysis by inhibiting the NF-KB and MAPK signaling," *Journal of Cellular Physiology*, vol. 234, no. 1, pp. 443–453, 2018.

[44] J. C. Xi, H. Y. Zang, L. X. Guo et al., "The PI3K/AKT cell signaling pathway is involved in regulation of osteoporosis," *Journal of Receptors and Signal Transduction*, vol. 35, no. 6, pp. 640–645, 2015.